World Journal of Advanced Engineering Technology and Sciences
eISSN: 2582-8266
Cross Ref DOI: 10.30574/wjaets
Journal homepage: https://wjaets.com/

(REVIEW ARTICLE)

Check for updates

Modeling of the human heart in 3D using DTI images

Ihab ELAFF *

Department of Computer Science and Engineering, College of Engineering, Qatar University, Qatar.

World Journal of Advanced Engineering Technology and Sciences, 2025, 15(02), 2450-2459

Publication history: Received on 13 April 2025; revised on 20 May 2025; accepted on 22 May 2025

Article DOI: https://doi.org/10.30574/wjaets.2025.15.2.0812

Abstract

Modeling the heart requires detailed representation of both the myocardial structure and the conduction system. Traditional CT and MRI imaging techniques fall short in capturing the anisotropic characteristics essential for accurate modeling of the heart's electrical and mechanical behaviors. This study employs Diffusion Tensor Magnetic Resonance Imaging (DT-MRI) to extract and model the myocardial fiber structure in a macroscopic domain. The diffusion properties are analyzed using scalar indices such as Mean Diffusivity, Fractional Anisotropy, and Diffusion Volume, enabling differentiation between myocardial and non-myocardial tissues. The dataset, acquired from a healthy subject, is processed using thresholding techniques to segment the myocardium and reconstruct a 3D heart model. The resulting anatomical model is integrated into a full human torso to enable forward modeling of the Body Surface Potential Map (BSPM). This study lays the groundwork for simulating cardiac excitation and paves the way for future inclusion of the conduction system.

Keywords: Diffusion Tensor MRI (DTI); Myocardium; Heart Modeling; 3D Heart Reconstruction

1. Introduction

Two main structures are of concern when modeling the heart, the Myocardium and the conduction system. In particular, the anatomical structure of the heart is obtained from medical images specially the CT-Scan and the MR images. However, modeling the heart using CT-scans or regular MRI will not be capable of providing the required level of detail, as the anisotropy of the tissues cannot be detected form such methods.

The heart Myocardium has strong anisotropic properties that affect both the electrical and the mechanical functions of the heart. Modeling the Myocardium as isotropic material is addressed in some models [1 – 5], but most of the other models consider the Myocardium as an anisotropic material.

In the anisotropic models of the heart, determination of the fibers structure information is accomplished by a variety of methods. One of the commonly used methods such as the work of Streeter et. al. [6] involves dissection information, where each voxel of the anatomical model of the heart is assigned to a local fibers direction [7 – 13]. Other models, such as the work of Nielson et. al. [14], assign fibers directions according to mathematical formulae [15 – 21]. The most recent models use the Diffusion Tensor MRI to obtain the fibers structure. Some models use the DTI for geometric reconstruction only [22, 23] while others employ the DTI data in the calculations of the Forward and the Inverse Problems [24 – 27].

With Diffusion Tensor Magnetic Resonance Imaging (DTI / DT-MRI), it is now possible to observe fine structures inside organs such as the structure of the brain and the structure of the heart. DTI was originally designed to determine the macrostructure of the brain, and for the heart it has been shown that DTI data have excellent correlation with dissection methods [28].

* Corresponding author: Ihab ELAFF. ORCID: 0000-0002-0913-5476

2. Methods

2.1. The Diffusion Tensor MRI

The operation of MRI scanners depends on the spinning properties of molecules [29]. The water molecules are usually considered by MRI devices and when a strong magnetic field is applied to the sample, water molecules align to spin parallel to this field. The molecules act as small magnets, and when a strong magnetic field is applied in the sample, they take one of the setting NN-SS, which is a weak relation, or NS-NS, which is a strong relation. Almost about 50% of water molecules in the sample are arranged in the first setting and 50% in the other setting. The MRI scanner sends a radio wave with a frequency that is equivalent to water molecules spinning (resonance) in a direction perpendicular to the strong magnetic field, which enable water molecules to gain some energy. The loosely arranged molecules (NN-SS) gain more energy than the strongly arranged ones (NS-NS). When the applied radio wave is turned off, then molecules that gained the energy lose this energy through the effect of the strong magnetic field. The loss of energy generates a signal that can be received by the MRI scanner (T1). When the strong magnetic field is turned off, another loss of energy can be observed as the water molecules restore their original state (T2).

The amount of water molecules in the sample affects the amplitude and the duration of the received signal and as water content inside biological tissues varies, grey-level image can be generated. The most used timing to produce the MR images is after the switching-off of the perpendicular radio wave (T1), as high contrast images between different tissues can be produced [29].

Tissues anisotropy affects the produced images, as the intensity of the received signal varies with different scanning angles in the same sample (vortex). This leads to the development of another MR imaging technique which is the Diffusion Weighted MRI (DW-MRI) [30]. The DW-MRI is accomplished by scanning a sample in three orthogonal directions and the mean of the received signals is calculated to produce a better representation to the amount of water molecules in the sample. This technique improves the quality of the MRI images, although it cannot provide the directional quantity of water molecules in the sample.

Another MRI imaging technique is the Diffusion Tensor MRI (DTI) where the scanning is accomplished for the sample in six directions. Basser et. al. [31] developed a model that is capable of describing the diffusion tensor in terms of three eigenvalues (diffusion coefficients) in the direction of three eigenvectors depending on the six images that are produced by the DTI scanner. This model considers the first eigenvector to be in the principal direction of diffusion and has the largest diffusion coefficient. As the largest amount of water will be in the longitudinal direction of cells, then the principle direction of diffusion, which has the largest diffusion coefficient, will be locally tangential to the fibers direction. This indicates that the amount of water molecules in a certain direction is directly related to the diffusion coefficient.

The scope of extracting cardiac fibers structure on a microscopic scale is very difficult, so it is modeled on a macroscopic scale by giving an average diffusion for a group of fibers in a certain space. Diffusion properties allow the classification of different types of tissues, and can be used for tissue segmentation; as it can provide unique micro-structural and physiological information for the sample [36].

2.2. The Diffusion Tensor (DT)

In three-dimensional space, the generalized diffusion tensor is a symmetric, positive definite, second-order 3 x 3 matrix. The three upper and lower off-diagonal elements are identical; Dxy = Dyx, Dxz = Dzx, and Dyz = Dzy. The diffusion tensor, D, as introduced by Basser et. al [98] therefore contains six unique elements.

$$D = \begin{bmatrix} D_{xx} & D_{xy} & D_{xz} \\ D_{yx} & D_{yy} & D_{yz} \\ D_{zx} & D_{zy} & D_{zz} \end{bmatrix} \qquad \text{……..(1)}$$

Because D is symmetric and positive definite, its three eigenvectors (principal coordinate directions) e1, e2, and e3 are orthogonal. Related to them are three positive eigenvalues (principal effective diffusivities), λ1, λ2, and λ3 with (λ1≥ λ2≥ λ3). Thus, the first (the largest) eigenvector gives the main diffusion direction, which corresponds to the fibers direction, and the other two eigenvectors will be the cross-fibers directions.

If

$$E = [\, e1 | e2 \mid e3 \,] \ldots\ldots\ldots\ldots (2)$$

and

$$\Lambda = \begin{bmatrix} \lambda_1 & 0 & 0 \\ 0 & \lambda_2 & 0 \\ 0 & 0 & \lambda_3 \end{bmatrix} \quad \ldots\ldots\ldots\ldots\ldots (3)$$

then

$$D = E\, \Lambda\, ET \quad \ldots\ldots\ldots\ldots\ldots (4)$$

where E is columns matrix of eigenvalues, and Λ is the diffusion coefficients matrix.

2.3. The DT Scalar Indices

The direction of the fibers varies from one location to another location, so rotational-invariant quantities are required to describe the diffusion of each element in the sample. Many methods are derived to provide rotational invariant quantities of diffusion. These include the Mean Diffusivity; the Rational Anisotropy; the Fractional Anisotropy; the Skewness; the Linear-anisotropy, Planner-anisotropy, and Isotropy [32 – 35].

The equation of the Mean Diffusivity is:

$$MD = \frac{1}{3}\sum_{i=1}^{3} \lambda_i \quad \ldots\ldots\ldots\ldots\ldots (5)$$

The equation of the Rational Anisotropy is:

$$RA = \frac{1}{6}\sqrt{\frac{\sum_{i=1}^{3}(\lambda_i - \overline{\lambda})^2}{\overline{\lambda}^2}} \quad \ldots\ldots\ldots\ldots (6)$$

where $\overline{\lambda}$ is the mean eigenvalue. The equation of the Fractional Anisotropy (FA) as presented by Basser et. al. is:

$$FA = \sqrt{\frac{3}{2}\frac{\sum_{i=1}^{3}(\lambda_i - \overline{\lambda})^2}{\sum_{i=1}^{3}\lambda_i^2}} \quad \ldots\ldots\ldots\ldots\ldots (7)$$

The equation of the Skewness is:

$$SK = \frac{1}{3}\sum_{i=1}^{3}(\lambda_i - \overline{\lambda})^3 \quad \ldots\ldots\ldots\ldots\ldots (8)$$

The equations of the Linear anisotropy, the Planar anisotropy and the Isotropy are:

$$C_L = \frac{\lambda_1 - \lambda_2}{\sum_{i=1}^{3} \lambda_i} \quad \text{.....(9)}$$

$$C_P = \frac{2(\lambda_2 - \lambda_3)}{\sum_{i=1}^{3} \lambda_i} \quad \text{.....(10)}$$

$$C_S = \frac{3\lambda_3}{\sum_{i=1}^{3} \lambda_i} \quad \text{.....(11)}$$

the Diffusion Volume (DV) quantity:

$$DV = \frac{4}{3}\pi.\lambda_1.\lambda_2.\lambda_3 \quad \text{..... (12)}$$

2.4. Data Acquisition

One of the most recent imaging technologies that has been used to determine Myocardium fibers structure is DTI [28]. The dataset used in this project was downloaded from the John Hopkins University website [36]. This dataset was taken for a male subject with no cardiac-disease history. Data were stored in 3D matrices of size 256 x 256 x 134 sample points (corresponding to 0.4297 x 0.4297 x 1.0 mm), where each vortex in the matrix consist of three eigenvectors of diffusion which represent the local fibers direction and cross-fibers directions as well as three eigenvalues of diffusion in the direction of each eigenvector in addition to an intensity map for each slice. Some of the DTI slices contain atrium data which is reduced by including the first 110 slices only. This dataset was stored as Matlab file format (.MAT). The work done has been implemented using the C++ programming language, which makes it necessary to decode these files.

The heart was placed in an acrylic container filled with Fomblin. Fomblin has a low dielectric effect and minimal MR signal thereby increasing contrast and eliminating unwanted susceptibility artifacts near the boundaries of the heart [36]. The low intensity components in the intensity map represent non-heart material as shown in Figure 1, where the dark areas of the shown Grayscale image represent the low intensity components. Very sharp edges exist between the heart material and the surrounding area where it was very clear to select a threshold value that separates between the two different areas.

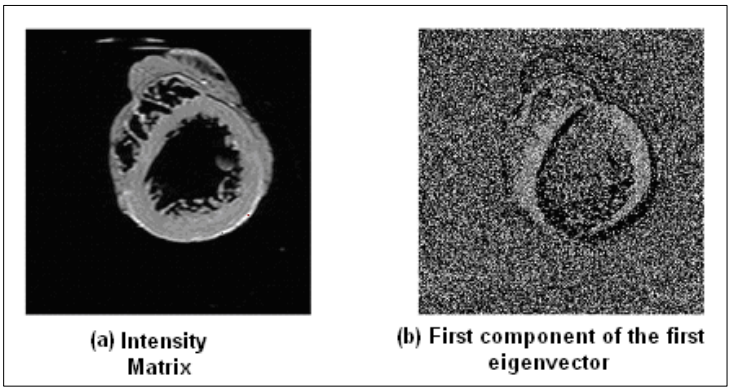

Figure 1 Grayscale preview of the intensity map (a) and colored image of the first component of the first eigenvector (b)

The first processing step was to take a threshold in each intensity map to produce a binary image that is used as a mask which applied to the corresponding slices of eigenvalues and eigenvectors to remove all low intensity components (Figure 2). This was a preparatory step to reduce the amount of eigenvalues and eigenvectors of each slice to the scope of the heart material as possible for the next phases of processing.

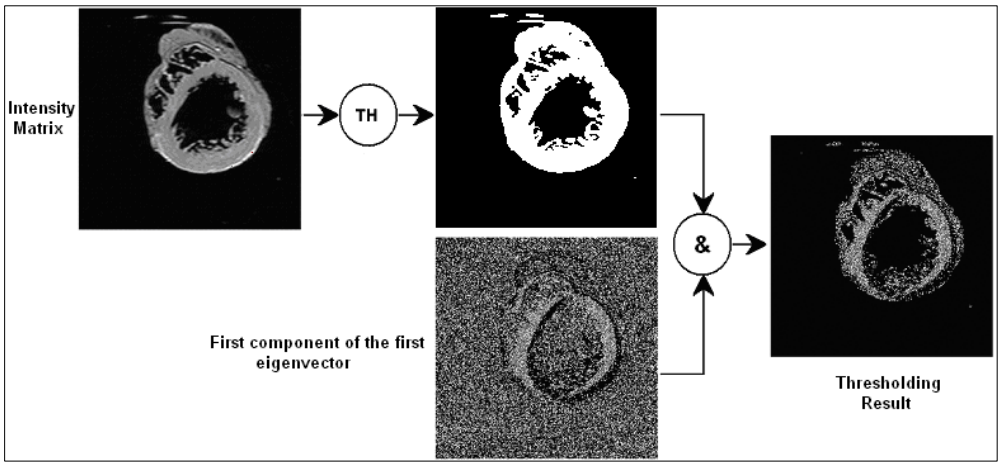

Figure 2 Intensity map is used to remove low intensity components from the first component of the first eigenvector

The heart material contains both excitable (Myocardium fibers, Purkinje fibers) and non-excitable (Epicardium wall, fat tissues, arteries … etc) materials. It was reported that similar microstructures would have similar diffusion coefficients in both longitudinal and traverse directions. Then, it is feasible to distinguish between different tissues and remove the undesired one from the domain. This step is necessary as the excitation propagates in the excitable materials only.

2.5. Extracting the Myocardium

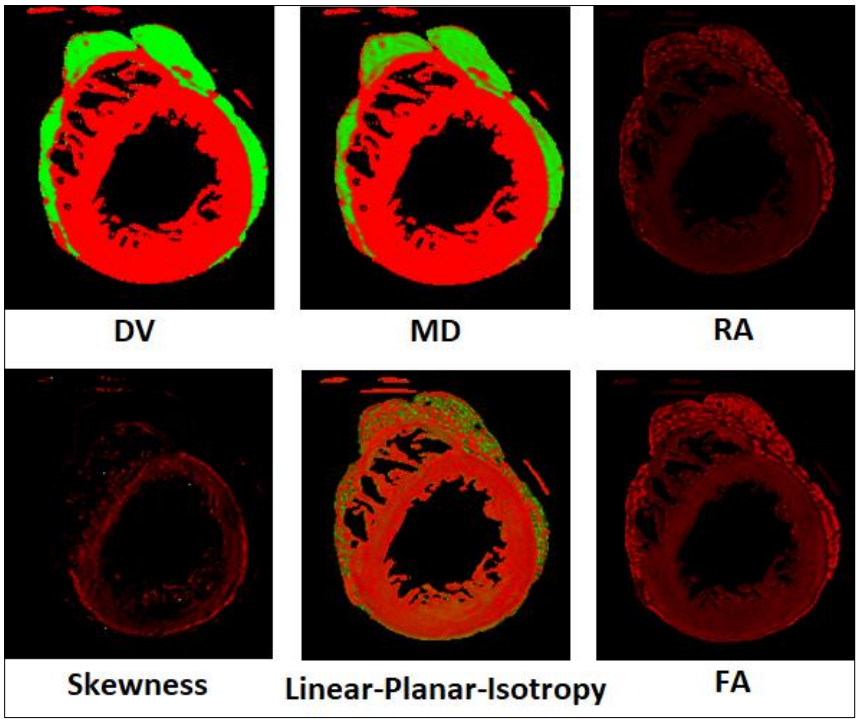

Figure 3 Rotational Invariant quantities for a heart slice

Removing of the Epicardium tissues manually is a very time consuming and subjected to errors. It will be very helpful to develop an automatic method that is capable of separating different tissues based on one of the rotational invariant quantities in addition to the biological and physiological facts of the heart tissues as well as the working methodology

of the DTI scanner. A variety of rotational invariant quantities of diffusion such as Diffusion Volume (DV), Mean Diffusivity (MD), Rational Anisotropy (RA), Fractional Anisotropy (FA), Skewness (SK), Linear anisotropy Planner anisotropy and Isotropy (CL, CP, CS) have been calculated from the DTI dataset and compared together (Figure 3).

The MRI is capable of showing low intensity areas for zones that contains low amount of water and vice versa [29, 30, 37, 38]. For example, during the time T1 it is found that muscular tissues will have higher intensity and longer decay time than in fats tissues, which indicates that the amount of water in the Myocardium is more than in fat tissues [37]. In regions where Purkinje cells contain more glycogen and less organelle than in normal cardiac cells then Purkinje cells intensity will be higher than in normal cardiac cells. Moreover, Epicardium and Endocardium walls have limited intercellular and extracellular fluids than in Myocardium wall as stated before, which indicate that these walls will have lower intensity than in the Myocardium. As the DV is directly related to the volume of water molecules in the sample, it can be used to differentiate between different tissues.

The full histogram (Figure 4 shows the part of histogram that contains largest peaks) derived from the DV map (this is normalized with respect to the mean intensity of elements in the half of the first peak and most of the second peak as they contains most of Myocardium tissues) shows that low intensity points, which represent most of Epicardium wall and fats tissues, are concentrated in the first peak (left) of the DV histogram. By testing different threshold values it is concluded that the first peak contains some of Myocardium tissues as well because of the macroscopic scale of the DT-MRI. The second peak represents mainly most of the Myocardium tissues and some of conduction system tissues. After the second peak, there is an almost flat line which represents the high intensity zones like blood vessels and some of conduction system zones.

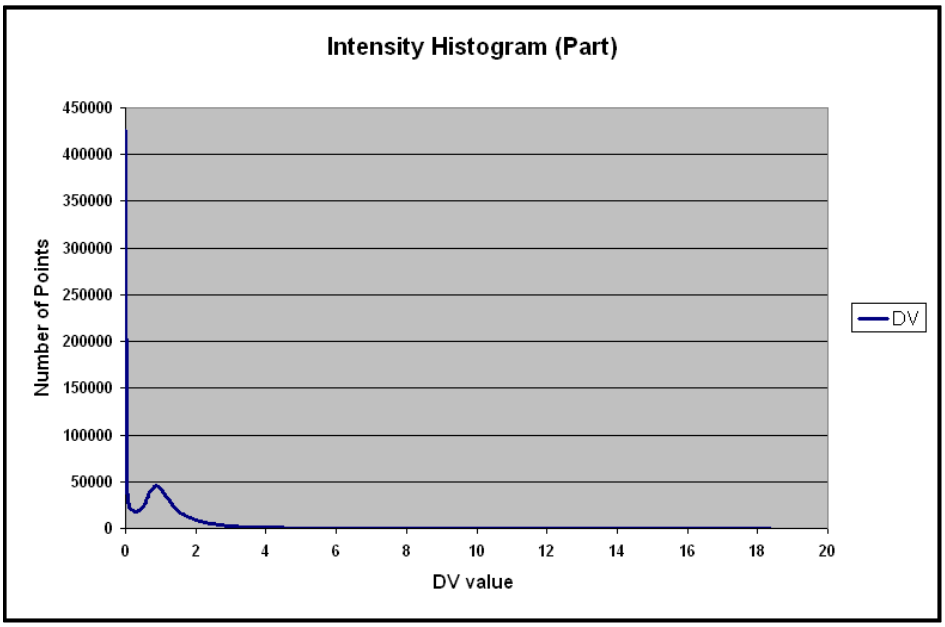

Figure 4 Intensity map histogram for the DV quantity

Thresholding values that capable of separating different structures are introduced in Table 1

Table 1 Thresholds of the DV intensities of different tissues

Tissue	DV Intensity (Normalized)
Fats & Epicardium	0.000 – 0.036
Myocardium	0.036 – 2.600
Purkinje Tissue	2.600 – 5.500
Others (e.g. blood)	>5.500

3. Results and discussion

The threshold has been chosen according to Table 1 to remove the Epicardium, the Endocardium the fat tissues, and other non-Myocardium tissues. The structure is generated after some manual segmentation as shown in Figure 5.

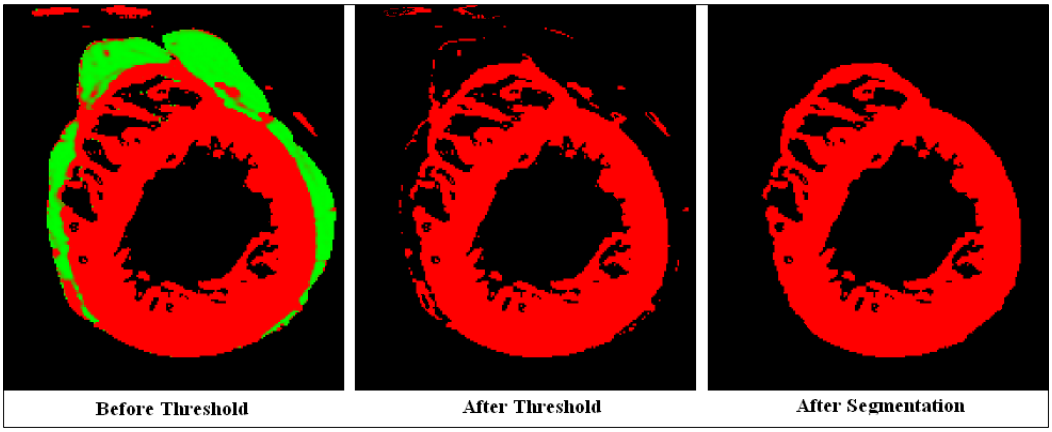

Figure 5 Removing Endocardium using DV quantity and fine-tuning by manual segmentation

Finally, the heart was reconstructed in 2 forms: the 1st one is as 3D volume matrix to model the excitation propagation and the 2nd one as a boundary surface for modeling the Body Surface Potential Map (BSPM) [39]. The LV and the RV cavities also reconstructed in the boundary surface model as blood volume in ventricles can affect the resultant BSPM. The heart is then inserted into the human torso [40] model with its proper location and orientation deduced from the CT-scan images of the modeled body and other anatomical references [30, 41, 42] (Figure 6).

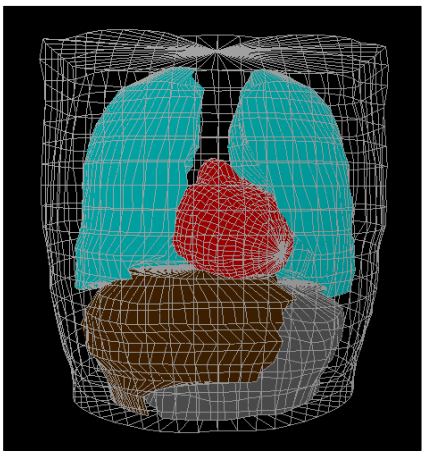

Figure 6 Complete Body torso with heart inserted in its proper location and orientation

Finally, the body torso is ready for modeling the BSPM (Figure 7), but there is still one detail which is the conduction system of the heart model; this is where the excitation propagation started and it will be in the next stage.

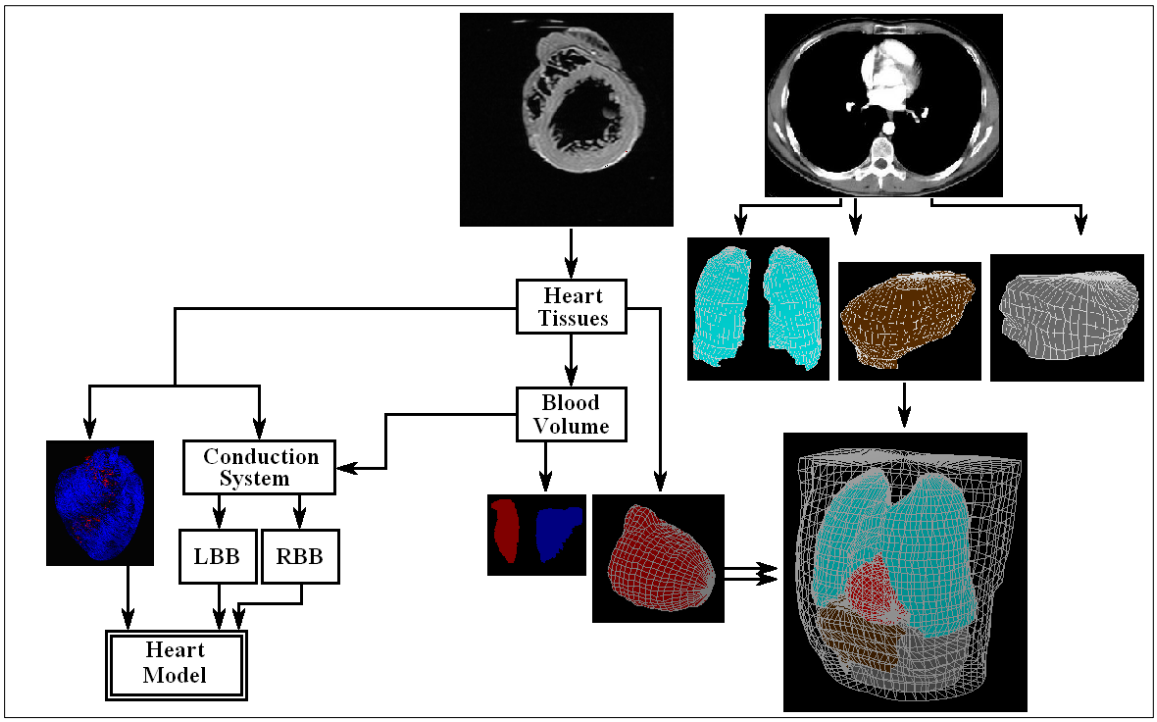

Figure 7 Block diagram of modeling the body and the heart after finishing the body model and the heart Myocardium model

4. Conclusion

This work demonstrates a reliable methodology for modeling the myocardium of the heart using DT-MRI data. By analyzing rotationally invariant diffusion tensor indices, it is possible to distinguish myocardial tissue from surrounding non-excitable tissues, achieving precise segmentation. The extracted myocardial structure was used to generate both volume and surface models suitable for further computational simulations. Integrating the heart model into a human torso enables realistic BSPM modeling. Although this study focused on the myocardial structure, future work will incorporate the conduction system to simulate complete cardiac excitation dynamics.

Compliance with ethical standards

Acknowledgments

Dr. Patrick A. Helm and Dr. Raimond L. Winslow at the Centre for Cardiovascular Bioinformatics and Modelling of John Hopkins University and Dr. Elliot McVeigh at the National Institute of Health for provision of DT-MRI data.

References

[1] A.E. Pollard and R.C. Barr "The Construction of an Anatomically Based Model of the Human Ventricular Conduction System" IEEE Trans. Biom. Eng. (1990); 37(12): 1173-1185.

[2] X. Zhang, I. Ramachandra, Z. Liu, B. Muneer, S.M. Pogwizd, and B. He "Noninvasive three-dimensional electrocardiographic imaging of ventricular activation sequence" Am J Physiol Heart Circ Physiol (2005); 289: H2724–H2732.

[3] T. Berger, G. Fischer, B. Pfeifer, R. Modre, F. Hanser,T. Trieb, F. X. Roithinger, M. Stuehlinger, O. Pachinger,B. Tilg, and F. Hintringer "Single-Beat Noninvasive Imaging of Cardiac Electrophysiology of Ventricular Pre-Excitation" J. Am. Coll. Cardiol. (2006);48:2045-2052.

[4] B.E. Pfeifer "Model-based segmentation techniques for fast volume conductor generation", Ph.D. Thesis, Institute of Biomedical Engineering, University for Health Sciences, Medical Informatics and Technology, Austria (2005).

[5] B. He, and D. Wu "Imaging and Visualization of 3-D Cardiac Electric Activity" IEEE Tran. Inf Tech. Biomed. 2001; 5(3): 181-186.

[6] F.P. Mall "On The Muscular Architecture of the Ventricles of the Human Heart" The American Journal of Anatomy (1911); vol. 11(3):211-266.

[7] K. Simeliusa, J. Nenonena, M. Horácekb "Modeling Cardiac Ventricular Activation" Inter. J. of Bioelectromagnetism, (2001); 3(2):51 - 58.

[8] B.H. Smaill, I.J. LeGrice, D.A. Hooks, A.J. Pullan, B.J. Caldwell and P.J. Hunter "Cardiac structure and electrical activation: Models and measurement" Proc. of the Australian Physiological and Pharmacological Society, (2004); 34: 141-149

[9] S.B. Knisley, N. Trayanova, and F. Aguel "Roles of Electric Field and Fibre Structure in Cardiac Electric Stimulation" Biophysical Journal, (1999); 77:1404–1417

[10] M. Lorange, and R. M. Gulrajani "A computer Heart Model Incorporating Anisotropic Propagation" Journal of Electrocardiology, (1993);26(4):245-261

[11] B. He, G.Li, and X. Zhang "Noninvasive Imaging of Cardiac Transmembrane Potentials Within Three-Dimensional Myocardium by Means of a Realistic Geometry Anisotropic Heart Model" IEEE Trans. Biomed. Eng. (2003); 50(10): 1190-1202.

[12] G. Li, X. Zhang, J. Lian, and B. He "Noninvasive Localization of the Site of Origin of Paced Cardiac Activation in Human by Means of a 3-D Heart Model" IEEE Trans. Biomed. Eng. (2003); 50(9): 1117-1120.

[13] Z. Liu, C. Liu, and B. He "Noninvasive Reconstruction of Three-Dimensional Ventricular Activation Sequence From the Inverse Solution of Distributed Equivalent Current Density" IEEE Trans. Med. Imag. (2006); 25(10): 1307-1318.

[14] P.M.F. Nielsen, I.J. Le Grice, B.H. Smaill, and P.J. Hunter "Mathematical model of geometry and fibrous structure of the heart" The Am. Phys. Soc. (1991); 260: H1365-H1378.

[15] L.W. Wang, H.Y. Zhang, P.C. Shi "Simultaneous Recovery of Three-dimensional Myocardial Conductivity and Electrophysiological Dynamics: A Nonlinear System Approach" Computers in Cardiology, (2006);33:45-48.

[16] O. Berenfeld and J. Jalife "Purkinje-Muscle Reentry as a Mechanism of Polymorphic Ventricular, Arrhythmias in a 3-Dimensional Model of the Ventricles" Circ. Res., (1998);82;1063-1077

[17] D.S. Farina, O. Skipa, C. Kaltwasser, O. Dossel and W.R. Bauer "Personalized Model of Cardiac Electrophysiology of a Patient" IJBEM (2005);7(1): 303-306

[18] M. Seger "Modeling the Electrical Function of the Human Heart", Ph.D. Thesis, Institute of Biomedical Engineering, University for Health Sciences, Medical Informatics and Technology, Austria (2006).

[19] O.G. Bernus "Development of a realistic computer model of the human ventricles for the study of reentrant arrhythmias" Ph.D. Thesis, University of Gent, Belgium (2003).

[20] C. Hintermuller "Development of a Multi-Lead ECG Array for Noninvasive Imaging of the Cardiac Electrophysiology", Ph.D. Thesis, Institute of Biomedical Engineering, University for Health Sciences, Medical Informatics and Technology,Austria, (2006)

[21] L. Cheng "Non-Invasive Electrical Imaging of the Heart", Ph.D. Thesis, The University of Auckland,New Zealand (2001).

[22] J.M. Peyrat, M. Sermesant, X. Pennec, H. Delingette, C. Xu, E. McVeigh and N. Ayache "Statistical Comparison of Cardiac Fibre Architectures", FIMH (2007); 4466: 413-423.

[23] L. Zhukov, A.H. Barr "Heart-Muscle Fibre Reconstruction from Diffusion Tensor MRI" VIS 2003. IEEE, (2003); Conf. Proc.: 597-602.

[24] D.F. Scollan "Reconstructing The Heart: Development and Application of Biophysically Based Electrical Models of Propagation in Ventricular Myocardium Reconstructed from DTMRI", Ph.D. Thesis, Johns Hopkins University (2002)

[25] R.L. Winslow, D.F. Scollan, J.L. Greenstein, C.K. Yung, W. Baumgartner, G. Bhanot, D.L. Gresh and B.E. Rogowitz "Mapping, modeling,and visual exploration of structure-function relationships in the heart" IBM Sys J.,(2001); 40(2):342-359.

[26] M. Sermesant, Y. Coudiere, H. Delingette, N. Ayache, J. Sainte-Marie,D. Chapelle, F. Clement and M. Sorine "Progress towards model-based estimation of the cardiac electromechanical activity from ECG signals and 4D images" ESAIM, 2002; 12: 153-162.

[27] M. Sermesant , H. Delingette, and N. Ayache "An Electromechanical Model of the Heart for Image Analysis and Simulation" IEEE Trans. Med. Imag. (2006); 25(5): 612-625.

[28] E.W. Hsu, A.L. Muzikant, S.A. Matulevicius, R.C. Penland and C.S. Henriquez "Magnetic Resonance Myocardial Fibre-Orientation Mapping with Direct Histological Correlation" Am. J. Physiol Heart Circ Physiol, (1998); 274:1627-1634.

[29] A.R. Margulis "Open Field Magnetic Resonance Imaging: Equipment, Diagnosis and Interventional Procedures" Springer-Verlag Telos, (2000); ISBN: 3-540-63781-8.

[30] D.D. Stark and W.G. Bradley "Magnetic Resonance Imaging" 3re Ed., C.V. Mosby, (1999); ISBN: 0-8151-8518-9.

[31] P.J. Basser, J. Mattiello and D. LeBihan "MR Diffusion Tensor Spectroscopy and Imaging" Biophys. J., (1994); 66: 259-267.

[32] A. Vilanova, S. Zhang, G. Kindlmann and D. Laidlaw "An Introduction to Visualization of Diffusion Tensor Imaging and Its Applications" Springer Berlin Heidelberg (2006), ISBN: 978-3-540-31272-7.

[33] P.J. Basser and C. Pierpaoli "Microstructural and Physiological Features of Tissues Elucidated by Quantitative-Diffusion-Tensor MRI" J. Magn. Reso., (1996); 111:209–219.

[34] I. ELAFF, I. A. EL-KEMANY, and M. KHOLIF "Universal and stable medical image generation for tissue segmentation (The unistable method)," Turkish Journal of Electrical Engineering and Computer Sciences: Vol. 25: No. 2, Article 32, 2017. https://doi.org/10.3906/elk-1509-100.

[35] I. Elaff, “Medical Image Enhancement Based on Volumetric Tissue Segmentation Fusion (Uni-Stable 3D Method)”, Journal of Science, Technology and Engineering Research, vol. 4, no. 2, pp. 78–89, 2023. https://doi.org/10.53525/jster.1250050.

[36] The Center for Cardiovascular Bioinformatics and Modeling, John Hopkins University Site "http://www.ccbm.jhu.edu/research/DTMRIDS.php", July 2011.

[37] R.B. Lufkin "The Mri Manual" 2nd Ed., C.V. Mosby, (1998); ISBN: 0-8151-5665-0.

[38] S.C. Bushong "Magnetic Resonance Imaging: Physical and Biological Principles" 3rd Ed., Mosby, (2003); ISBN: 0-323-01485-2.

[39] I. ELAFF (2018) "Modeling of realistic heart electrical excitation based on DTI scans and modified reaction diffusion equation," Turkish Journal of Electrical Engineering and Computer Sciences: Vol. 26: No. 3, Article 2. https://doi.org/10.3906/elk-1710-118J

[40] I. ELAFF “Modeling of 3D Inhomogeneous Human Body from Medical Images”, World Journal of Advanced Engineering Technology and Sciences. 2025, 15(02): 2010-2017. https://doi.org/10.30574/wjaets.2025.15.2.0772

[41] F.W. Sears, M.W. Zemansky and H.D. Young "University Physics", 6th Ed., Addison-Wesley Pub. co., (1982), ISBN:0-201-07199-1.

[42] A. Timmis and S. Brecker "Diagnoses in Color: Cardiology" Times Intr. Pub. Ltd., (1997), ISBN: 0-7234-25515.